Inorganic Chemistry

Article

pubs.acs.org/IC

Axial Ligand Coordination to the C−H Amination Catalyst $Rh_2(esp)_2$: A Structural and Spectroscopic Study

Evan Warzecha, Timothy C. Berto, and John F. Berry*

Department of Chemistry, University of Wisconsin−Madison, 1101 University Avenue, Madison, Wisconsin 53706, United States

Supporting Information

ABSTRACT: The compound $Rh_2(esp)_2$ (esp = α,α,α′,α′-tetramethyl-1,3-benzenediproponoate) is the most generally effective catalyst for nitrenoid amination of C−H bonds. However, much of its fundamental coordination chemistry is unknown. In this work, we study the effects of axial ligand coordination to the catalyst $Rh_2(esp)_2$. We report here crystal structures, cyclic voltammetry, UV−vis, IR, Raman, and ^{1}H NMR spectra for the complexes $Rh_2(esp)_2L_2$ where L = pyridine, 3-picoline, 2,6-lutidine, acetonitrile, and methanol. The compounds all show well-defined $\pi^* \rightarrow \sigma^*$ electronic transitions in the 16500 to 20500 cm^{-1} range, and Rh−Rh stretching vibrations in the range from 304 to 322 cm^{-1}. Taking these data into account we find that the strength of axial ligand binding to $Rh_2(esp)_2$ increases in the series $CH_3OH \sim$ 2,6-lutidine < CH_3CN < 3-methylpyridine ∼ pyridine. Quasi-reversible $Rh_2^{4+/5+}$ redox waves are only obtained when either acetonitrile or no axial ligand is present. In the presence of pyridines, irreversible oxidation waves are observed, suggesting that these ligands destabilize the Rh_2 complex under oxidative conditions.

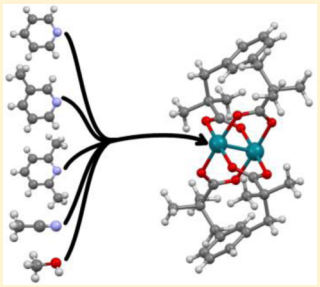

INTRODUCTION

Dirhodium tetracarboxylate complexes play a prominent role in catalysis and have been especially intensively studied for their ability to promote reactions resulting in the functionalization of C−H bonds.[1−6] The dirhodium tetraacetate derivative $Rh_2(esp)_2$, **1** (esp = α,α,α′,α′-tetramethyl-1,3-benzenediproponoate), was first designed as a selective and efficient C−H amination catalyst by the Du Bois group in 2004.[7] Since then, it has become an enabling catalyst for a number of advances in synthetic organic chemistry including intra- and intermolecular C−H aminations.[5,8,9] The C−H amination reactions have been widely utilized and studied, but they are mechanistically quite complex. While traditional kinetic studies have been hampered by an apparent zero-order dependence on the Rh_2 catalyst,[8,10] electrochemical and in situ spectroscopic studies have suggested that there are multiple catalytically active species.[11−13] In separate studies, we have explored chemical alteration of the esp ligand backbone leading in general to comparable catalytic capability toward intramolecular C−H amination but partial loss of activity in intermolecular C−H amination.[14,15] Previous studies have suggested that C−H amination can occur via sequential proton coupled electron transfer steps, which could potentially be performed electrochemically.[11] The possibility of performing C−H amination electrocatalytically led us to study the electrochemistry of **1** in the presence of amine substrates and 2,6-lutidine as a "non-coordinating base".[11] However, our electrocatalytic efforts have been stymied by very low currents. Recognizing that 2,6-lutidine can in fact coordinate to $Rh_2(OAc)_4$,[16] we wondered if 2,6-lutidine could be binding to **1** and inhibiting catalysis. Although thermodynamic information exists for axial ligand binding to other dirhodium carboxylates,[17−20] comparable data do not exist for **1**. We decided to undertake an exploratory study of **1** in the presence of various pyridine and nonpyridine axial liagnds. Our further efforts toward electrocatalysis will be reported elsewhere. We note that pyridine adducts of other Rh_2 complexes supported by chelating dicarboxylate ligands have been reported,[21] but only structural data are available for these compounds. Five ligands - pyridine, 3-methylpyridine, 2,6-lutidine, acetonitrile, and methanol - are evaluated in this study, and the corresponding complexes are investigated by X-ray crystallography, UV−visible absorption, infrared, NMR, and confocal Raman spectroscopies. Each of these ligands forms a complex of the general formula $Rh_2(esp)_2L_2$ where L = pyridine (**2**), 3-methylpyridine (**3**), 2,6-lutidine (**4**), MeCN (**5**), or MeOH (**6**), as shown in Chart 1. We describe here the trends in axial ligand binding and how the physical properties of the Rh_2 complex are affected.

EXPERIMENTAL SECTION

All reagents were obtained commercially and used without further purification unless otherwise noted. Reactions were performed using

Chart 1. Complexes Described in This Study

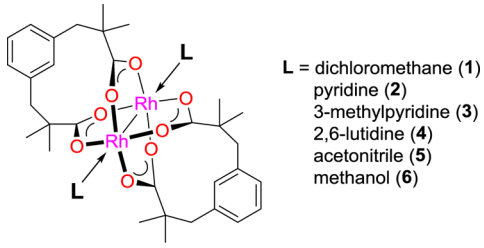

Received: July 9, 2015
Published: August 26, 2015

DOI: 10.1021/acs.inorgchem.5b01532
Inorg. Chem. 2015, 54, 8817−8824

oven-dried glassware under an atmosphere of nitrogen using Schlenk techniques. Dichloromethane was dried over CaH_2 and distilled prior to use. 2,6-Lutidine was dried over $AlCl_3$ and distilled prior to use. Pyridine was dried over CaH_2 and distilled prior to use.

^{1}H NMR spectra were obtained using a Bruker 400 MHz Avance spectrometer at room temperature. UV/vis spectra were obtained in real-time using a Miniature BLUE- Wave UV/vis dip probe with a Tungsten–Krypton light source and a 10 mm path length tip. IR spectra were obtained using a PIKE Technologies MIRacle ATR setup mounted in a Bruker Vertex 70 spectrometer. Raman spectra were obtained at room temperature on crystalline samples using a Thermo Fisher DXR Raman microscope with 532 nm excitation wavelength. Cyclic voltammetry was performed using 10–20 mL dichloromethane solutions containing 0.1 M tetrabutylammonium hexaflorophosphate with 0.0025 M analyte under a nitrogen atmosphere. The electrodes consisted of a Pt coil working electrode, a Pt wire counter electrode, and a reference electrode made of a silver wire in a 0.01 M Ag^+ solution contained by a Vycor tip. Measurements were taken using a BAS Epsilon potentiostat.

$Rh_2(esp)_2$ was synthesized according to a previously published method.[7] $Rh_2(esp)_2L_2$ complexes with L = pyridine, acetonitrile, and 3-methylpyridine were prepared by dissolving **1** in a solution of 10:1 DCM/L and crystallizing by addition of hexanes. $Rh_2(esp)_2L_2$ complexes with L = methanol and 2,6-lutidine were synthesized by dissolving **1** in neat L followed by recrystallization by slow evaporation.

Crystals for X-ray crystallography were selected under oil at ambient conditions. Crystals were attached to the tip of a MiTeGen MicroMount, mounted in a stream of cold nitrogen at 100(1) K, and centered in the X-ray beam using a video monitoring system. Crystal evaluation and data collection were performed on a Bruker Quazar SMART APEX-II diffractometer with Cu Kα (λ = 1.541 78 Å; **3**, **6**) or Mo Kα (λ = 0.710 73 Å; **2**, **4**, and **5**) radiation. The data were collected using a routine to survey an entire sphere of reciprocal space and indexed by the SMART program, and the structures were solved via direct methods and refined by iterative cycles of least-squares refinement on F^2 followed by difference Fourier synthesis.[22] All H atoms were included in the final structure factor calculation at idealized positions and allowed to ride on the neighboring atoms with relative isotropic displacement coefficients.

$Rh_2(esp)_2(py)_2$ (**2**). Anal. Calcd for $Rh_2(esp)_2(py)_2{\cdot}CH_2Cl_2$: C 51.56, H 5.23, N 2.80. Found: C 51.99, H 5.21, N 3.07. ^{1}H NMR (CD_2Cl_2, 400 MHz, ppm): δ 0.82 (24H, s), 2.50 (8H, s), 6.71 (4H, d), 6.94 (2H, s), 6.94 (2H, t), 8.69 (12H, d), 7.68 (6H, t), 7.33 (12H, t). Raman (cm^{-1}): 116, 140, 331, 629, 656, 1012, 1074, 1215, 1598, 2929, 2984, 3059, 3070. IR (ATR, cm^{-}1): 662 m, 665 m, 648 w, 693 s, 711 m, 746 m, 772 w, 779 w, 800 w, 824 w, 882 w, 906 w, 932 w, 1007 w, 1034 w, 1070 w, 1133 w, 1204 w, 1213 w, 1247 w, 1266 w, 1322 w, 1374 w, 1410 m, 1439 w, 1447 w, 1476 w, 1586 s, 2871 w, 2923 w, 2959 w, 2972 w, 2988 w, 3054 w.

$Rh_2(esp)_2(3\text{-methylpyridine})_2$ (**3**). Anal. Calcd for $Rh_2(esp)_2(3\text{-methylpyrine})_2$: C 55.93, H 5.72, N 2.97. Found: C 55.60, H 5.64, N 2.93. ^{1}H NMR (CD_2Cl_2, 400 MHz, ppm): δ 0.92 (24H, s), 2.48 (6H, s), 2.59 (8H, s), 6.80 (4H, d), 7.00 (2H, s), 7.03 (2H, t), 8.44 (2H, s), 8.40 (2H, d), 7.50 (2H, d), 7.19 (2H, q). Raman (cm^{-1}): 133, 323, 643, 807, 1000, 1031, 1043, 1089, 1595, 2917, 2969, 3063. IR (ATR, cm^{-1}): 630 m, 648 w, 701 m, 713 m, 751 w, 770 w, 778 w, 788 w, 881 w, 909 w, 927 w, 940 w, 1030 w, 1048 w, 1107 w, 1133 w, 1193 w, 1241 w, 1262 w, 1357 w, 1371 w, 1407 s, 1445 s, 1475 m, 1558 s, 2863 s, 2919 m, 2945 w, 2960 w, 2970 w, 2990 w, 3024 w.

$Rh_2(esp)_2(lut)_2$ (**4**). Anal. Calcd for $Rh_2(esp)_2(Lut)_2$: C 56.79, H 5.97, N 2.88. Found: C 55.61, H 5.91, N 2.75. Raman (cm^{-1}): 124, 161, 238, 277, 304, 440, 724, 833, 1268, 1287, 1451, 2923, 2945, 2973, 2986, 3059. IR (ATR, cm^{-1}): 633 m, 655 w, 668 w, 710 m, 734 w, 750 w, 768m, 775 m, 825 w, 882 w, 907 w, 927 w, 935 w, 1115 w, 1130 w, 1160 w, 1204 w, 1239 w, 1262 w, 1358 w, 1375 w, 1409 s, 1456 w, 1475 m, 1496 w, 1580 s, 2866 w, 2923 m, 2955 m, 2978 m.

$Rh_2(esp)_2(MeCN)_2$ (**5**). Anal. Calcd for $Rh_2(esp)_2(MeCN)_2$: C 51.43, H 5.48, N 3.33. Found: C 51.20, H 5.54, N 3.11. ^{1}H NMR (CD_2Cl_2, 400 MHz, ppm): δ 0.94 (24H, s), 1.97 (300H, s), 2.60 (8H, s), 6.81 (4H, d), 6.92 (2H, s), 7.04 (2H, t). Raman (cm^{-1}): 115, 150, 176, 316, 325, 749, 831, 834, 1003, 1239, 1370, 2271, 2303, 2931, 2950, 2965, 2981, 3057. IR (ATR, cm^{-1}): 623 m, 635 m, 657 w, 696 s, 709 s, 749m, 771 w, 780 w, 799 w, 824 w, 882 w, 906 w, 932 w, 1007 w, 1034 w, 1071 w, 1131 w, 1213 w, 1246 w, 1267 m, 1355 m, 1375 m, 1406 s, 1437 w, 1445 m, 1476 m, 1584 s, 2868 w, 2924 m, 2952 m, 2975 m′, 2988 m, 3056 w.

$Rh_2(esp)_2(MeOH)_2$ (**6**). Anal. Calcd for $Rh_2(esp)_2(MeOH)_2{\cdot}0.4CH_2Cl_2$: C 48.24, H 5.74. Found: C 48.29, H 5.50. ^{1}H NMR (d_4-MeOD, 400 MHz, ppm): δ 0.98 (24H, s), 2.62 (8H, s), 6.82 (4H, d), 7.00 (2H, s), 7.01 (2H, t). Raman (cm^{-1}): 107, 124, 153, 165, 171, 253, 290, 310, 443, 746, 828, 940, 1003, 1158, 1194, 1238, 1319, 1454, 1585, 2921, 2954, 2964, 2972, 3057. IR (ATR, cm^{-1}) 633 m, 658 w, 706 m, 747 w, 769 w, 778 w, 796 w, 817 w, 825 w, 883 w, 906 w, 925 w, 935 w, 1026 m, 1038 m, 1135 w, 1062 w, 1200 w, 1245 m, 1267 m, 1323 w, 1359 m, 1378 m, 1409 s, 1435 w, 1477 m, 1576 s, 2829 w, 2920 m, 2952 m, 2978 m, 3060 w, 3410 br, m.

RESULTS

Recrystallization of **1** in the presence of various axial ligands provides ready access to $Rh_2(esp)_2(L)_2$ compounds **2**–**6**. Interestingly, even the sterically hindered 2,6-lutidine forms a bis-adduct. Crystal structures of these compounds are shown in Figure 1, with the corresponding crystallographic data given in Tables 1 and 2. All of the compounds are centrosymmetric such that the phenylene rings of the two esp ligands are parallel to each other. While the variance in the Rh–Rh distance is limited to 0.044 Å, the lutidine adduct has a Rh–Rh distance 0.014 Å longer than the other pyridine adducts. The lutidine adduct **4**

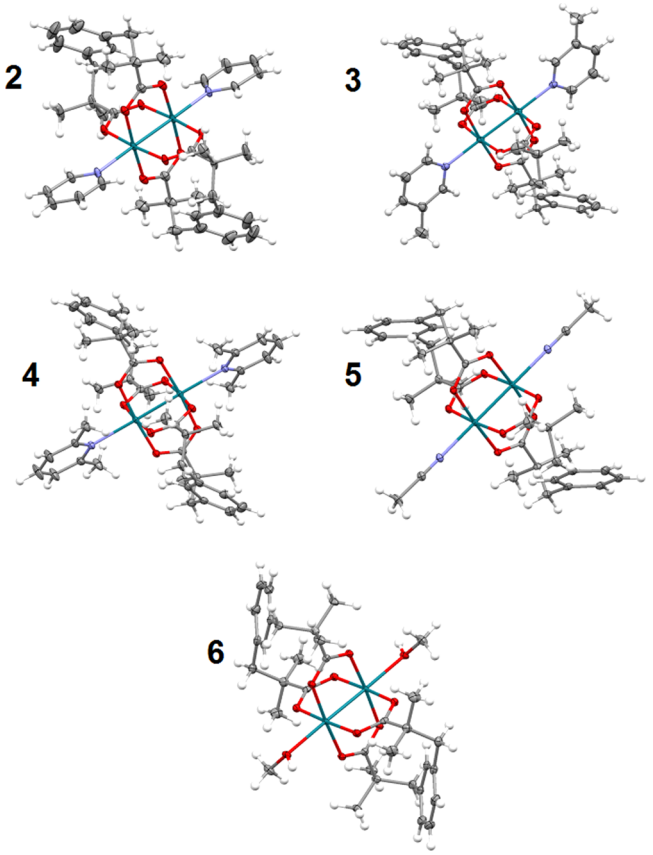

Figure 1. Crystallographically determined structures of **2**–**6** with thermal ellipsoids set at the 50% probability level. The Rh atoms are cyan, N atoms are blue, O atoms are red, C atoms are gray, and H atoms are white.

DOI: 10.1021/acs.inorgchem.5b01532
Inorg. Chem. 2015, 54, 8817–8824

Table 1. Crystal Data for 2−6

	2·CH_2Cl_2	3	4	5·2CH_2Cl_2	6·7/8CH_2Cl_2· 1/8CH_3OH
formula	$C_{43}H_{52}Cl_2N_2O_8Rh_2$	$C_{44}H_{54}N_2O_8Rh_2$	$C_{46}H_{58}N_2O_8Rh_2$	$C_{38}H_{50}Cl_4N_2O_8Rh_2$	$C_{35}H_{50.25}Cl_{1.75}O_{10.13}Rh_2$
λ	0.71073	1.54178	0.71073	0.71073	0.71073
cryst syst	monoclinic	monoclinic	triclinic	monoclinic	triclinic
space group	$C2/c$	$P2_1/c$	$P\bar{1}$	$P2_1/n$	$P\bar{1}$
a	18.3780(7)	10.2303(3)	10.828(3)	9.888(3)	11.624(1)
b	10.4361(4)	20.4927(7)	11.342(3)	15.882(4)	11.9813(8)
c	23.1475(8)	11.1999(4)	18.180(4)	13.728(3)	15.6522(9)
α	90	90	83.81(1)	90	100.665(6)
β	94.490(1)	114.096(1)	85.788(9)	92.222(5)	91.507(6)
γ	90	90	77.087(9)	90	115.278(4)
V	4425.9(3)	2143.4(1)	2160.7(9)	2154(1)	1923.4(2)
Z	4	2	2	2	2
P	1.503	1.464	1.495	1.558	1.555
R1,[a] wR2[b] [$I > 2\sigma(I)$]	0.0259, 0.0612	0.0227, 0.0609	0.0357, 0.0889	0.0174, 0.0426	0.0189, 0.0459
R1,[a] wR2[b] (all data)	0.0280, 0.0625	0.0239, 0.0618	0.0430, 0.0930	0.0190, 0.0436	0.0192, 0.0461

[a] $R1 = \sum||F_o| - |F_c||/[\sum|F_o|]$. [b] $wR2 = \{\sum[w(F_o^2 - F_c^2)^2]/[\sum[w(F_o^2)^2]]\}^{1/2}$, $w = 1/\sigma^2(F_o^2) + (aP)^2$, where $P = [\max(0 \text{ or } F_o^2) + 2(F_c^2)]/3$.

Table 2. Selected Bond Distances for 2−6

	Rh−Rh (Å)	Rh−L_{axial} (Å)	Rh−O_{av} (Å)
2	2.4023(2)	2.246(1)	2.037(1)
3	2.4057(3)	2.250(1)	2.041(1)
4[a]	2.4206(6)	2.413(2)	2.0388(2)
4[b]	2.4189(7)	2.386(3)	2.0412(2)
5	2.3920(7)	2.218(1)	2.0413(9)
6[a]	3.3769(3)	2.276(1)	2.039(1)
6[b]	3.3750(2)	2.319(1)	2.035(1)

[a,b] a and b refer to the two crystallographically independent molecules in the unit cell for **4** and **6**.

has not only the longest Rh−Rh distance, 2.4206(6) Å, but also the longest Rh−N bond distance, 2.413(2) Å. The latter is understandably due to the steric profile of the axial ligand, but it is interesting that the Rh−Rh bond is apparently flexible enough to elongate in order to accommodate the long Rh−N bonds. The remaining Rh−L_{axial} bond lengths fall in the close range of 2.218(1) Å, for **5**, to 2.319(1) Å, for **6**. Both **4** and **6** have two crystallographically independent molecules in their structures. In **4**, the two structures are distinguished by the orientation of the 2,6-lutidine ligand. In the first unit, the plane of the pyridyl unit of 2,6-lutidine bisects the molecule such that an entire esp ligand lies on each side of the plane. In the second unit, the plane of the 2,6-lutidine ligands is rotated by 90°, leaving two half esp ligands on each side of the plane. This difference in conformation has a small effect on the bond distances, most significantly on the Rh−L_{Axial} distance, which is 0.026 Å longer in the first unit. Compound **6** also displays two different orientations of the axial MeOH ligands. These orientations are rotated by 60° relative to each other. Similar to **4**, there is a significant difference in the Rh−L_{Axial} distances of 0.043 Å between the two conformers.

The previously reported 2,6-lutidine-$Rh_2(OAc)_4$ complex is stabilized by weak interactions between the oxygen atoms of acetate ligands and the methyl groups of lutidine.[16] In this study, nearly identical C···O distances are seen when OAc is replaced with the esp ligand. The through-space C···O distances are 3.017(4)−3.109(5) Å in **4a** and 2.952(4)−3.147(4) Å in **4b**, which compare favorably to the reported values of 3.073(7)−3.118(7) Å for the $Rh_2(OAc)_4$ complex.[16]

The ^{1}H NMR spectra for each of these complexes could not be obtained in the same solvent. Due to solubility issues, the pyridine adduct ^{1}H NMR spectrum could be obtained only in CD_2Cl_2. The 3-methylpyridine and acetonitrile adducts were also measured in CD_2Cl_2, but the methanol and 2,6-lutidine adducts do not remain bound at reasonable concentrations in most solvents. The ^{1}H NMR spectrum of **6** was obtained in d_4-MeOD; detection of bound methanol was not possible due to rapid exchange with the bulk solvent. For the weakly binding 2,6-lutidine ligand, a bis-adduct can be obtained in solution, as evidenced by UV−vis spectroscopy (vide infra). However, this bis-adduct requires the addition of so much lutidine (>10 equiv) that the esp signals cannot be seen by ^{1}H NMR spectroscopy.

Each compound measured has five ^{1}H NMR signals corresponding to the protons of the esp ligand, as shown in Chart 2. Of the aromatic signals, **a** is a one-proton triplet that

Chart 2. Esp Ligand with Proton NMR Assignments

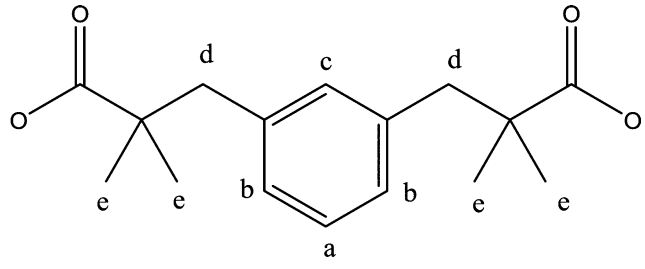

appears between 7.01 ppm in **6** and 7.04 ppm in **5**, **b** is a two-proton doublet that appears between 6.82 ppm in **6** and 6.80 in **2**, and **c** is a one-proton singlet that varies between 7.02 ppm in **2** and 6.92 ppm in **5**. The signal corresponding to **d** is a four-proton singlet that appears between 2.58 ppm in **3** and 2.62 ppm in **6**, while **e** is a 12-proton singlet that varies between 0.90 in **2** and 0.98 in **5** and **6**. When the axial ligand changes, the spectral changes are minor and the most significant change in the esp proton chemical shifts is the position of proton **c**, with a range of 0.10 ppm. Interestingly, in compounds **2** and **6** the signals for **a** and **c** overlap; however, in compounds **3** and **5** the singlet is distinct.

Attempts were made to determine the stability constants for axial ligand binding in compounds **2**−**6**; however these were

DOI: 10.1021/acs.inorgchem.5b01532
Inorg. Chem. 2015, 54, 8817−8824

stymied by the strong binding of the pyridines and acetonitrile and an inability to observe singly bound methanol and 2,6-lutidine complexes. Nevertheless, a relative stability trend was determined by systematically adding aliquots of the other ligands to solutions of compounds **2**–**6**. Using this method, a solution of **6** in methanol or **4** in 2,6-lutidine was completely converted to **5** with two equivalents of acetonitrile. Complex **5** in a solution of DCM was easily converted to **2** or **3** by the addition of either pyridine or 3-methylpyridine. Using these experiments we were able to determine the stability trend shown below.

$$\text{Methanol} \approx \text{2,6-Lutidine} < \text{Acetonitrile} < \text{Pyridine} \approx \text{3-Methylpyridine}$$

Binding constants that have been determined for $Rh_2(OAc)_4$, $Rh_2(TFA)_4$, and $Rh_2(O_2C_4H_7)$ with pyridine and acetonitrile reflect the trend we see here, with the pyridine binding constant being several orders of magnitude stronger than that of acetonitrile.[17−20] Additionally, when ligands similar to intramolecular C−H amination substrates such as 2,2,2-trichloroethyl sulfamate are examined, they bind even more weakly than methanol and 2,6-lutidine.

The electronic structures, and thus colors, of these complexes are highly sensitive to the identity of the axial ligand. This is due to perturbation of the Rh−Rh $\pi^* \rightarrow \sigma^*$ HOMO−LUMO transition by the axial ligands.[23] In CH_2Cl_2 solution, **1** appears green in color with an absorption maximum at 665 nm. Each of the potential axial ligands studied here causes a shift in this band to higher energy. Even the addition of the sterically demanding 2,6-lutidine causes a shift in the $\pi^* \rightarrow \sigma^*$ band, consistent with the binding of lutidine in solution, although >10 equiv of lutidine are required to observe this change. This result complements studies on $Rh_2(OAc)_4$ where 2,6-lutidine was also shown to bind crystallographically,[16] but for which spectral characterization was lacking. Figure 2 shows the UV−visible absorption spectra of all of the $Rh_2(esp)_2$ adducts studied here. In each case, the lowest energy band is ascribed to the $\pi^* \rightarrow \sigma^*$ HOMO−LUMO transition. The higher energy bands in the spectra are much less sensitive to changes in the identity of the axial ligand, in agreement with their assignment as $\pi^* \rightarrow$ Rh−O σ^*. Similar to the case of $Rh_2(OAc)_4$,[24] spectral changes may be analyzed taking into account the π and σ donor/acceptor characteristics of each ligand. In general, more strongly σ donating ligands will create a larger HOMO/LUMO gap by raising the energy of the σ^* LUMO, as will be discussed further in more quantitative terms (vide infra).

Of the $Rh_2(esp)_2L_2$ species investigated, the weakly binding ligands 2,6-lutidine and MeOH shift the $\pi^* \rightarrow \sigma^*$ transition to 599 and 596 nm, respectively. With the somewhat stronger binding ligand CH_3CN, this band shifts to 562 nm. The much stronger binding ligands pyridine and 3-methylpyridine shift the band to 520 and 523 nm, respectively, indicating that the addition of a slightly electron-donating *meta*-methyl group to the pyridine ligand does not significantly alter this ligand's interaction with the Rh_2 σ^* or π^* orbitals. These results contrast strongly with the lutidine spectrum. In accordance with their similar electronic substitutions, pyridine and 3-methylpyridine have nearly identical effects on the UV−vis spectrum of $Rh_2(esp)_2$, while 2,6-lutidine, however, is a measurably weaker donor. This effect is undoubtedly due to the steric hindrance of this ligand, which prevents it from interacting as strongly with the Rh−Rh center as the other pyridine derivatives.

Both FT-IR and Raman spectroscopies were employed in an effort to characterize the vibrational spectra of the $Rh_2(esp)_2L_2$ complexes **2**–**6**. In general, the FT-IR spectra are nearly identical, showing bands characteristic of the esp ligand (see Figure S1). Confocal Raman microscopy was used to obtain complementary vibrational data. By using an excitation wavelength of 532 nm, it is possible to provide resonance enhancement to vibrational bands coupled to the Rh_2 $\pi^* \rightarrow \sigma^*$ transition. Thus, while the IR spectra of **2**–**6** are very similar, the Raman spectrum for each compound is unique, as shown in Figure 3. Only the MeCN- and 2,6-lutidine-bound complexes have unique signals that may be attributable to their axial ligands, such as the C≡N stretch of **5** observed at 2271 cm^{-1}. These data are shown in Figure 3, where vibrational features

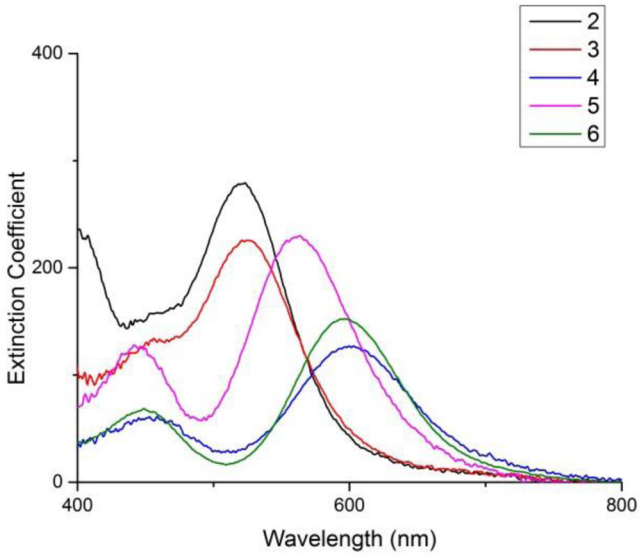

Figure 2. Absorption spectra of $Rh_2(esp)_2L_2$ recorded in CH_2Cl_2 with L = 3-methylpyridine (**3**), 2,6-lutidine (**4**), acetonitrile (**5**), methanol (**6**), and pyridine (**2**).

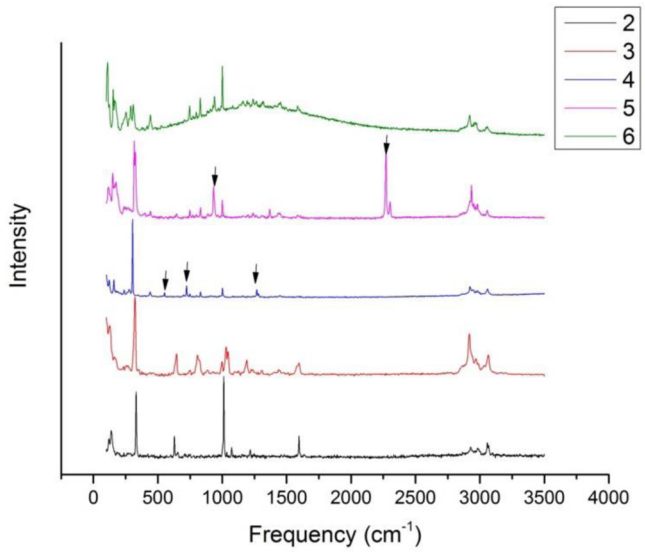

Figure 3. Raman spectra of compounds **1**–**6**. Peaks corresponding to unique axial ligand signals are indicated with a black arrow.

DOI: 10.1021/acs.inorgchem.5b01532
Inorg. Chem. 2015, 54, 8817−8824

associated with the given axial ligand are indicated with an arrow.

Of prime interest in the Raman spectra are signals corresponding to the Rh−Rh stretching frequencies, which to date have been measured for relatively few compounds.[25−33] These vibrations are known to occur at ∼300 cm^{-1}, but care must be taken in the assignment, since Rh−O stretches may also occur in this region.[34] By judiciously exciting the $\pi^* \rightarrow \sigma^*$ electronic transition rather than the higher energy $\pi^* \rightarrow$ Rh−O σ^* band, the Rh−Rh stretching features should be selectively resonance-enhanced. Interestingly, we are unable to assign a signal to the Rh−Rh vibration in the methanol-bound compound. In this compound, there are signals at 290 and 310 cm^{-1}; however the 290 cm^{-1} signal is likely a combination band of the 165 and 125 cm^{-1} signals, and the 310 cm^{-1} signal is the first overtone of the 155 cm^{-1} signal. The acetonitrile-bound complex has two bands, at 325 and 316 cm^{-1}, each of which might be the Rh−Rh stretch. However, the 325 cm^{-1} signal is likely a combination band from the 175 and 150 cm^{-1} bands, leaving the 316 cm^{-1} frequency assignable to the Rh−Rh stretch. The signals corresponding to the Rh−Rh vibrations for compounds **2**−**5** are shown in Table 3. Also in Table 3 are the

Table 3. Rh−Rh Bond Distances and Stretching Frequencies for Compounds 1−6 and Other Known Rh_2 Tetracarboxylate Compounds

axial ligand	Rh−Rh stretch, cm^{-1}	Rh−Rh distance, Å	ref
MeCN	316	2.3920(7)	this work
2,6-lutidine	304	2.4206(6)[a]	this work
2,6-lutidine	304	2.4189(7)[b]	this work
pyridine	331	2.4023(2)	this work
3-methylpyridine	322	2.4057(3)	this work
MeOH	N/A	3.3769(3)[a]	this work
MeOH	N/A	3.3750(2)[b]	this work
$Rh_2(OAc)_4$			
PPh_3	289	2.4505(2)	28
$AsPh_3$	297	2.427(1)	34, 55
$SbPh_3$	307	2.421(4)	55
MeCN	344	2.384(1)	56
H_2O	340	2.3855(5)	57, 58
$Rh_2(CHO_2)_4$			
PPh_3	286	2.451(4)	28

[a,b]a and b refer to the two crystallographically independent molecules in the unit cell for **4** and **6**.

existing Raman data for the known compounds that have been crystallographically characterized. Further support for our assignment of these Raman signals to the Rh−Rh stretches is supported by a Badger's rule analysis using the equation

$$r = \frac{C}{\nu^{2/3}} + d$$

where r is the Rh−Rh bond distance, ν is the Rh−Rh stretching frequency, and C and d are constants specific to the bond in question. A correlation plot is shown in Figure 4. The other known Rh_2 carboxylate complexes that have been studied by Raman spectroscopy and crystallography have been included in this table as well. Thus, the $Rh_2(OAc)_4$ compounds with the axial ligands H_2O, MeCN, PPh_3, $AsPh_3$, and $SbPh_3$ as well as $Rh_2(O_2CH)_4(PPh_3)_2$[34] were added to enhance the reliability in the trend.

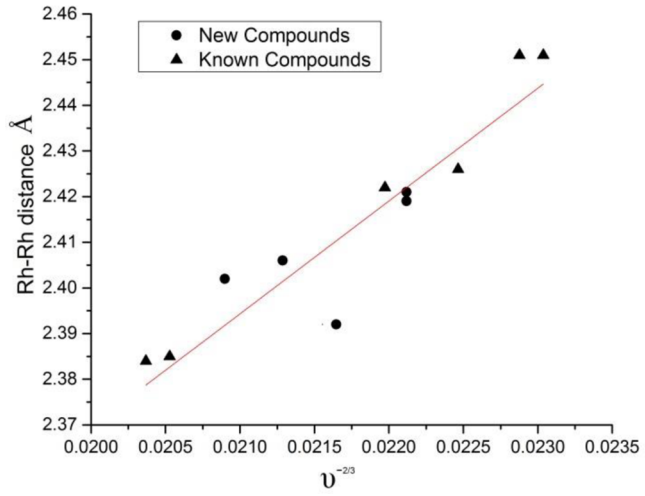

Figure 4. Badger's rule plot of the inverse stretching frequency against Rh−Rh distance. The linear fit is made using C = 24.1 ± 9.7 Å $cm^{2/3}$ and d = 1.89 ± 0.21 Å.

Cyclic voltammograms of compounds **1**−**6**, all measured in CH_2Cl_2, are shown in Figure 5. The electrochemical features of

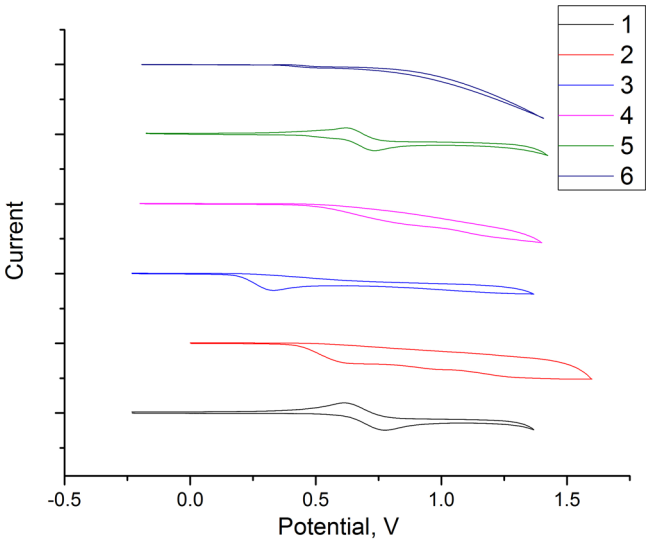

Figure 5. Cyclic voltammograms of **1**−**6** measured in DCM solution at room temperature with a scan rate of 100 mV/s. Potential is referenced to Fc/Fc^+.

these compounds are quite surprisingly varied. While **1** and **2** show (quasi)reversible waves that are easily assigned to the $Rh_2^{4+/5+}$ redox wave, the other compounds show generally more complex features. The pyridine derivatives show multi-electron irreversible features consistent with the occurrence of an irreversible chemical transformation upon oxidation from Rh(II) to Rh(III). This behavior is most likely due to the oxidative cleavage of the Rh−Rh bond, resulting in monometallic Rh(III) compounds, which would be too kinetically inert and thermodynamically stable to be re-reduced back to the Rh_2^{4+} state. In support of this proposal, Doyle and co-workers have characterized a number of Rh_2(III,III) species with strong axial donors in which the Rh−Rh bond has been severed.[35−39] Compound **6** shows an irreversible multielectron feature most likely due to MeOH oxidation. These results highlight the fact that discrete $[Rh_2(esp)_2]^+$ complexes having

DOI: 10.1021/acs.inorgchem.5b01532
Inorg. Chem. 2015, 54, 8817−8824

an oxidized Rh_2(II,III) core are stable and accessible only in certain circumstances. CH_2Cl_2 and acetonitrile appear to stabilize the Rh_2^{5+} state, whereas in the presence of pyridine ligands this oxidation state is not stable.

DISCUSSION

The general form of the d orbital manifold for Rh_2 carboxylates is shown in Figure 6. Binding of an axial ligand generally involves a major effect and a minor effect on this MO diagram. The major effect is the donation of the filled axial ligand lone pair orbitals into the Rh_2 σ^* MO, which then becomes destabilized. This interaction increases the $\pi^* \rightarrow \sigma^*$ gap, which in turn raises the energy of the primary absorption band in the UV−vis spectrum. The donation into the σ^* orbital weakens the Rh−Rh bond, increasing its length. The minor effect on the MO diagram is the stabilization of the π^* orbitals through π back-bonding. A strong π-accepting axial ligand would thus also cause a shift in the $\pi^* \rightarrow \sigma^*$ transition to higher energy, but removal of Rh_2 π^* electron density is expected to strengthen the Rh−Rh bond.

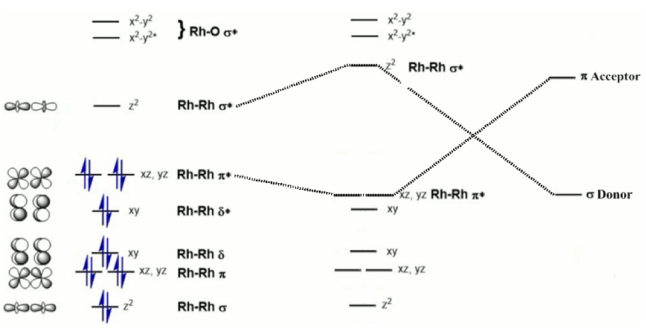

Figure 6. General molecular orbital diagram of Rh_2 carboxylates and the effect of binding σ-donor and π-acceptor ligands.

In the compounds studied here, several trends emerge. As the Rh−L_{ax} distance becomes shorter, the energy of the $\pi^* \rightarrow \sigma^*$ transition increases (see Table 4). Since a shorter Rh−L_{ax} distance leads to better orbital overlap, this agrees with our suggestion that the σ donation effect is the major contributor to the increase in the energy of the absorption maxima. Moreover, as shown in Figure 7, a quantitative linear correlation may be made between the $\pi^* \rightarrow \sigma^*$ transition energy and the Rh−L_{ax} distance, normalized to take into account the differences in L_{ax} atomic radii (the formal shortness ratio (FSR) method is used here).[40] Using this correlation, the $\pi^* \rightarrow \sigma^*$ transition energy of ∼15 000 cm^{-1} for **1** in CH_2Cl_2 suggests that CH_2Cl_2 does not coordinate to **1** in solution since a crystallographically characterized Rh_2−CH_2Cl_2 complex has a Rh−Cl bond distance of 2.65 Å,[41] corresponding to an FSR of 1.18.

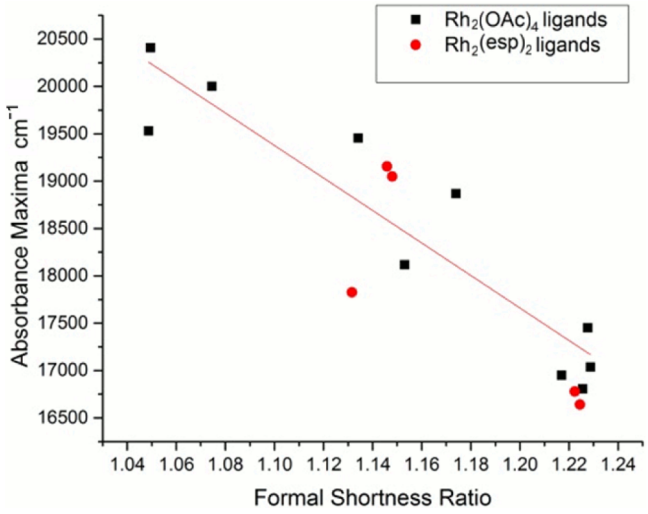

Figure 7. Plot of formal shortness ratio vs absorbance maxima. A combined set of $Rh_2(esp)_2$ and $Rh_2(OAc)_4$ complexes is shown.

The relative σ-donor strengths of the ligands studied may be found by looking at the FSR of the Rh−L_{axial} bond, which produces the following trend:

Methanol ≈ 2,6-Lutidine < Pyridine ≈ 3-Methylpyridine < Acetonitrile

However, this trend is not completely representative of the strength of axial ligand binding and does not match our

Table 4. Rh−L Bond Distances, Corresponding FSRs, and Energies for the Rh_2 $\pi^* \rightarrow \sigma^*$ Transition for Rh_2 Tetracarboxylate Compounds

	Rh−L_{ax} bond distance, Å	single bond covelent radii,[40] Å	Rh−L_{ax} formal shortness ratio	absorbance maxima, cm^{-1}	ref
$Rh_2(OAc)_4$ Complexes					
H_2O	2.310(3)	1.88	1.22	17 000	59, 60
PPh_3	2.477(1)	2.36	1.05	20 000	24
diethylamine	2.301(6)	1.96	1.17	18 900	61
DMF (*O* bound)	2.296(3)	1.88	1.23	17 500	62
MeOH	2.288(3)	1.88	1.22	16 900	63
Py	2.223(2)	1.96	1.13	19 500	46, 60
lutidine	2.402(4)	1.96	1.23	16 800	16
ACN	2.258(6)	1.96	1.15	18 100	56, 60
DMSO (*S*-bound)	2.451(1)	2.28	1.07	20 000	60, 64
$AsPh_3$	2.576(1)	2.46	1.05	19 500	55
$Rh_2(esp)_2$ Complexes					
ACN	2.2184(11)	1.96	1.13	17 800	this work
MeOH	2.2976(12)	1.88	1.22	16 800	this work
Py	2.2457(13)	1.96	1.15	19 200	this work
3-methylPy	2.2502(17)	1.96	1.15	19 000	this work
Lut	2.3995(2)	1.96	1.22	16 600	this work

DOI: 10.1021/acs.inorgchem.5b01532
Inorg. Chem. 2015, 54, 8817−8824

qualitative assessment given earlier. This is because acetonitrile, which has the shortest Rh−L_{axial} bond length, is easily displaced by the pyridines in solution. This anomalously short Rh−N bond is due to the increased s character of the acetonitrile lone pair, which results in a weaker but shorter bond. The possibility of π back-bonding from the Rh_2 π^* orbitals into the C−N π^* levels could also be considered here, but there are no indicators that this interaction is important. The C≡N stretching frequency in **5**, 2271 cm^{-1}, is very close to that of free acetonitrile (2267 cm^{-1}).[42−45]

Another potential measure of the strength of axial ligand binding develops as we consider the *trans* influence of each axial ligand: How do the different axial ligands affect the strength of the Rh−Rh bond? In this case, the data in Table 3 and Figure 4 are useful to analyze. In general, a strong Rh−L_{axial} bond is expected to elongate the Rh−Rh distance. Indeed, this is what is seen in our data, as the compounds with the shortest Rh−Rh distances, **5** and **6**, are the ones with the most labile axial ligands (CH_3CN and MeOH, respectively). However, the longest Rh−Rh distance in this series corresponds to the complex of the weakly binding 2,6-lutidine ligand. This anomaly, along with the unusual trend in Rh−Rh stretching frequencies (which incorrectly predicts pyridine to be the weakest axial ligand!), suggests more nuance to this simple model. A possible explanation for the unusually high Rh−Rh stretching frequencies of the pyridine adducts is that these ligands could engage in π back-bonding to the Rh_2 unit, effectively removing electron density from the Rh−Rh π^* orbitals. Previous crystallographic examination of the pyridine adduct of $Rh_2(OAc)_4$ by Koh and Christoph in 1978 provided no evidence for such an interaction.[46] Furthermore, an in-depth experimental/computational study of a pyridine complex of a related Ru_2(II,II) system has afforded no evidence of Ru_2 π^* back-bonding.[47] The more likely explanation for the tighter correlation between normalized Rh−L_{axial} bond lengths and axial ligand binding is that a deeper potential energy well exists for the Rh−L_{axial} bond than for the Rh−Rh bond. Unusually shallow potential energy wells have been encountered before for metal−metal-bonded systems, but these have mainly been for examples containing first-row transition metals, where wide variations in metal−metal bond distances are more routinely observed.[48−52] However, similar observations on second-row complexes have been made,[53,54] but to our knowledge this is the first evidence for a shallow Rh−Rh potential energy well in the tetracarboxylate family.

The coordination of axial ligands to $Rh_2(esp)_2$ and the stability of the resulting adducts are of significant relevance to catalysis. Once bound, the pyridines are difficult to replace or remove. This means that pyridines can poison the catalyst in multiple ways. Binding to the catalyst and blocking the active site is one such mechanism; it is observed even in the sterically hindered 2,6-lutidine and seems to be irreversible in the case of pyridine and 3-methylpyridine. Under oxidizing conditions, $Rh_2(esp)_2$ shows irreversible electrochemical features consistent with the decomposition of the catalyst into Rh(III) fragments when in the presence of pyridines, including the weakly coordinating 2,6-lutidine.

CONCLUSION

We have examined the effect of coordinating five ligands to the catalyst $Rh_2(esp)_2$ on the electronic, vibrational, and NMR spectra as well as on the crystal structures and electrochemistry. We found links between the electronic spectra and Rh−axial ligand distance, which when normalized using the formal shortness ratio, are consistent with the molecular orbital model provided above, where stronger σ donation weakens the Rh−Rh bond and increases the $\pi^* \rightarrow \sigma^*$ gap. Useful vibrational data were obtained with Raman experiments, with which we were able to assign a Rh−Rh stretching frequency consistent with the Rh−Rh bond distance using Badger's rule, with the exception of the methanol-bound complex, which does not seem to have a Raman signal corresponding to the Rh−Rh stretch. Cyclic voltammetry revealed that pyridines may inhibit oxidative catalysis by promoting the cleavage of the Rh−Rh bond and deactivating the catalyst under oxidative conditions, as well as with their generally strong binding, which may inhibit the binding of substrate.

ASSOCIATED CONTENT

Supporting Information

The Supporting Information is available free of charge on the ACS Publications website at DOI: 10.1021/acs.inorgchem.5b01532.

Figures S1 through S5 contains the IR and NMR spectra for compounds **2**−**6** (PDF)
Crystallographic files (CIF)

AUTHOR INFORMATION

Corresponding Author

*E-mail: berry@chem.wisc.edu.

Notes

The authors declare no competing financial interest.

ACKNOWLEDGMENTS

We thank the U.S. Department of Energy, Office of Science, Basic Energy Sciences, Catalysis Science Program, for support of this work (DE-FG02-10ER16204), and we are grateful to Brian Dolinar for crystallographic assistance.

REFERENCES

(1) Davies, H. M. L.; Manning, J. R. *Nature* **2008**, *451*, 417−424.
(2) Davies, H. M. L.; Morton, D. *Chem. Soc. Rev.* **2011**, *40*, 1857−1869.
(3) Davies, H. M. L.; Beckwith, R. E. J. *Chem. Rev.* **2003**, *103*, 2861−2904.
(4) Doyle, M. P.; Duffy, R.; Ratnikov, M.; Zhou, L. *Chem. Rev.* **2010**, *110*, 704−724.
(5) Kornecki, K. P.; Powers, D. C.; Ritter, T.; Berry, J. F. *Prog. Inorg. Chem.*; John Wiley & Sons, Inc: Hoboken, 2014; Vol. *58*.
(6) Du Bois, J. *Org. Process Res. Dev.* **2011**, *15*, 758−762.
(7) Espino, C. G.; Fiori, K. W.; Kim, M.; Du Bois, J. *J. Am. Chem. Soc.* **2004**, *126*, 15378−15379.
(8) Fiori, K. W.; Du Bois, J. *J. Am. Chem. Soc.* **2007**, *129*, 562−568.
(9) Roizen, J. L.; Harvey, M. E.; Du Bois, J. *Acc. Chem. Res.* **2012**, *45*, 911−922.
(10) Fiori, K. W.; Espino, C. G.; Brodsky, B. H.; Du Bois, J. *Tetrahedron* **2009**, *65*, 3042−3051.
(11) Kornecki, K. P.; Berry, J. F. *Chem.−Eur. J.* **2011**, *17*, 5827−5832.
(12) Zalatan, D. N.; Du Bois, J. *J. Am. Chem. Soc.* **2009**, *131*, 7558−7559.
(13) Perry, R. H.; Cahill, T. J.; Roizen, J. L.; Du Bois, J.; Zare, R. N. *Proc. Natl. Acad. Sci. U. S. A.* **2012**, *109*, 18295−18299.
(14) Kornecki, K. P.; Berry, J. F. *Eur. J. Inorg. Chem.* **2012**, *2012*, 562−568.
(15) Kornecki, K. P.; Berry, J. F. *Chem. Commun.* **2012**, *48*, 12097−12099.

DOI: 10.1021/acs.inorgchem.5b01532
Inorg. Chem. 2015, 54, 8817−8824

(16) Aoki, K.; Inaba, M.; Teratani, S.; Yamazaki, H.; Miyashita, Y. *Inorg. Chem.* **1994**, *33*, 3018−3020.
(17) Drago, R. S.; Long, J. R.; Cosmano, R. *Inorg. Chem.* **1982**, *21*, 2196−2202.
(18) Drago, R. S.; Long, J. R.; Cosmano, R. *Inorg. Chem.* **1981**, *20*, 2920−2927.
(19) Drago, R. S.; Tanner, S. P.; Richman, R. M.; Long, J. R. *J. Am. Chem. Soc.* **1979**, *101*, 2897−2903.
(20) Trindade, A. F.; Coelho, J. A. S.; Afonso, C. A. M.; Veiros, L. F.; Gois, P. M. P. *ACS Catal.* **2012**, *2*, 370−383.
(21) Bonar-Law, R. P.; McGrath, T. D.; Singh, N.; Bickley, J. F.; Femoni, C.; Steiner, A. *J. Chem. Soc., Dalton Trans.* **2000**, 4343−4347.
(22) Sheldrick, G. M. *Acta Crystallogr., Sect. A: Found. Crystallogr.* **2008**, *64*, 112−122.
(23) Berry, J. F. *Dalton Trans.* **2012**, *41*, 700−713.
(24) Christoph, G. G.; Halpern, J.; Khare, G. P.; Koh, Y. B.; Romanowski, C. *Inorg. Chem.* **1981**, *20*, 3029−3037.
(25) Miskowski, V. M.; Dallinger, R. F.; Christoph, G. G.; Morris, D. E.; Spies, G. H.; Woodruff, W. H. *Inorg. Chem.* **1987**, *26*, 2127−2132.
(26) Clark, R. J. H.; Hempleman, A. J.; Flint, C. D. *J. Am. Chem. Soc.* **1986**, *108*, 518−520.
(27) Clark, R. J. H.; Hempleman, A. J. *Inorg. Chem.* **1988**, *27*, 2225−2229.
(28) Clark, R. J. H.; Hempleman, A. J. *Inorg. Chem.* **1989**, *28*, 746−752.
(29) Best, S. P.; Clark, R. J. H.; Nightingale, A. J. *Inorg. Chem.* **1990**, *29*, 1383−1387.
(30) Clark, R. J. H.; Hempleman, A. J. *Inorg. Chem.* **1989**, *28*, 92−96.
(31) Best, S. P.; Chandley, P.; Clark, R. J. H.; McCarthy, S.; Hursthouse, M. B.; Bates, P. A. *J. Chem. Soc., Dalton Trans.* **1989**, 581−588.
(32) Clark, R. J. H.; West, D. J.; Withnall, R. *Inorg. Chem.* **1992**, *31*, 456−459.
(33) Clark, R. J. H.; Hempleman, A. J. *J. Chem. Soc., Dalton Trans.* **1988**, *61*, 313−329.
(34) Cotton, F. A.; Murillo, C. A.; Walton, R. A. *Multiple Bonds between Metal Atoms*, 3rd ed.; Springer Science and Business Media, Inc.: New York, 2005.
(35) Angelone, D.; Draksharapu, A.; Browne, W. R.; Choudhuri, M. M. R.; Crutchley, R. J.; Xu, X.; Xu, X.; Doyle, M. P. *Inorg. Chim. Acta* **2015**, *424*, 235−240.
(36) Xie, J.-H.; Zhou, L.; Lubek, C.; Doyle, M. P. *Dalton Trans.* **2009**, 2871−2877.
(37) Wolf, J.; Poli, R.; Xie, J.-H.; Nichols, J.; Xi, B.; Zavalij, P.; Doyle, M. P. *Organometallics* **2008**, *27*, 5836−5845.
(38) Xie, J.-H.; Nichols, J. M.; Lubek, C.; Doyle, M. P. *Chem. Commun.* **2008**, 2671−2673.
(39) Nichols, J. M.; Wolf, J.; Zavalij, P.; Varughese, B.; Doyle, M. P. *J. Am. Chem. Soc.* **2007**, *129*, 3504−3505.
(40) Pyykkö, P.; Atsumi, M. *Chem. - Eur. J.* **2009**, *15*, 186−197.
(41) Kornecki, K. P.; Briones, J. F.; Boyarskikh, V.; Fullilove, F.; Autschbach, J.; Schrote, K. E.; Lancaster, K. M.; Davies, H. M. L.; Berry, J. F. *Science* **2013**, *342*, 351−354.
(42) Venkateswarlu, P. *J. Chem. Phys.* **1951**, *19*, 293−298.
(43) Venkateswarlu, P. *J. Chem. Phys.* **1952**, *20*, 923−923.
(44) Milligan, D. E.; Jacox, M. E. *J. Mol. Spectrosc.* **1962**, *8*, 126−133.
(45) Marzocchi, M. P.; Dobos, S. *Spectrochim. Acta Part A: Molecular Spectroscopy* **1974**, *30*, 1437−1444.
(46) Koh, Y. B.; Christoph, G. G. *Inorg. Chem.* **1978**, *17*, 2590−2596.
(47) Brown, T. R.; Dolinar, B. S.; Hillard, E. A.; Clérac, R.; Berry, J. F. *Inorg. Chem.* 10.1021/acs.inorgchem.5b01241.
(48) Rohmer, M.-M.; Strich, A.; Bénard, M.; Malrieu, J.-P. *J. Am. Chem. Soc.* **2001**, *123*, 9126−9134.
(49) Rohmer, M.-M.; Bénard, M. *J. Am. Chem. Soc.* **1998**, *120*, 9372−9373.
(50) Benbellat, N.; Rohmer, M.-M.; Bénard, M. *Chem. Commun.* **2001**, 2368−2369.
(51) Hall, M. B. *Polyhedron* **1987**, *6*, 679−684.
(52) Wagner, F. R.; Noor, A.; Kempe, R. *Nat. Chem.* **2009**, *1*, 529−536.
(53) Petrie, S.; Stranger, R. *Inorg. Chem.* **2004**, *43*, 2597−2610.
(54) Stranger, R.; Turner, A.; Delfs, C. D. *Inorg. Chem.* **2001**, *40*, 4093−4100.
(55) Clark, R. J. H.; Hempleman, A. J.; Dawes, H. M.; Hursthouse, M. B.; Flint, C. D. *J. Chem. Soc., Dalton Trans.* **1985**, 1775−1780.
(56) Cotton, F. A.; Thompson, J. L. *Acta Crystallogr., Sect. B: Struct. Crystallogr. Cryst. Chem.* **1981**, *37*, 2235−2236.
(57) Dikarev, E. V.; Shpanchenko, R. V.; Andreini, K. W.; Block, E.; Jin; Petrukhina, M. A. *Inorg. Chem.* **2004**, *43*, 5558−5563.
(58) Cotton, F. A.; DeBoer, B. G.; LaPrade, M. D.; Pipal, J. R.; Ucko, D. A. *Acta Crystallogr., Sect. B: Struct. Crystallogr. Cryst. Chem.* **1971**, *27*, 1664−1671.
(59) Martin, D. S.; Webb, T. R.; Robbins, G. A.; Fanwick, P. E. *Inorg. Chem.* **1979**, *18*, 475−478.
(60) Johnson, S. A.; Hunt, H. R.; Neumann, H. M. *Inorg. Chem.* **1963**, *2*, 960−962.
(61) Koh, Y. B.; Christoph, G. G. *Inorg. Chem.* **1979**, *18*, 1122−1128.
(62) Moszner, M.; Glowiak, T.; Ziolowski, J. J. *Polyhedron* **1985**, *4*, 1413−1417.
(63) Noinville, V.; Viossat, B.; Dung, N.-H. *Acta Crystallogr., Sect. C: Cryst. Struct. Commun.* **1993**, *49*, 1297−1298.
(64) Cotton, F. A.; Felthouse, T. R. *Inorg. Chem.* **1980**, *19*, 323−328.

DOI: 10.1021/acs.inorgchem.5b01532
Inorg. Chem. 2015, 54, 8817−8824